İSTANBUL UNIVERSITY CERRAHPAŞA

ORIGINAL ARTICLE
Electrica 2024; 24(1): 109-118

Detection of Alzheimer's Dementia by Using Deep Time–Frequency Feature Extraction

Ozlem Karabiber Cura[1], H. Sabiha Ture[2], Aydin Akan[3]

[1]Department of Biomedical Engineering, Izmir Katip Celebi University Faculty of Engineering and Architecture, Izmir, Turkey
[2]Department of Neurology, Izmir Katip Celebi University Faculty of Medicine, Izmir, Turkey
[3]Department of Electrical and Electronics Engineering, Izmir University of Economics Faculty of Engineering, Izmir, Turkey

†Cite this article as: O. Karabiber Cura, H. S. Ture, A. Akan, "Detection of alzheimer's dementia by using deep time-frequency feature extraction," *Electrica*, 24(1), 109-118, 2024.

ABSTRACT

Alzheimer's disease (AD), a neurological condition connected with aging, causes cognitive deterioration and has a substantial influence on a patient's daily activities. One of the most widely used clinical methods for examining how AD affects the brain is the electroencephalogram (EEG). Handcraft calculating descriptive features for machine learning algorithms requires time and frequently increases computational complexity. Deep networks provide a practical solution to feature extraction compared to handcraft feature extraction. The proposed work employs a time–frequency (TF) representation and a deep feature extraction-based approach to detect EEG segments in control subjects (CS) and AD patients. To create EEG segments' TF representations, high-resolution synchrosqueezing transform (SST) and traditional short-time Fourier transform (STFT) approaches are utilized. For deep feature extraction, SST and STFT magnitudes are used. The collected features are classified using a variety of classifiers to determine the EEG segments of CS and AD patients. In comparison to the SST method, the STFT-based deep feature extraction strategy produced improved classification accuracy between 79.56% and 92.96%.

Index Terms—Alzheimer's dementia, electroencephalogram (EEG), synchrosqueezing transform (SST), short-time Fourier transform (STFT), time–frequency analysis, deep feature extraction.

I. INTRODUCTION

Memory loss, difficulty locating words and languages, lack of desire, cognitive slowness, planning problems, and changes in conscious awareness levels are all indicators of dementia [1–3]. This condition is caused by a number of reasons, some more prevalent than others [1]. Alzheimer's disease (AD) is the most common dementia kind, contributing to around 60%-70% of dementia occurrences in those over the age of 65 [4]. The extracellular buildup of the protein fragment β-amyloid peptide (Aβ) and the creation of an aberrant version of tau protein within neurons are two of the most commonly observed brain abnormalities associated with AD.

This causes nerve cell death, which manifests as small memory issues that escalate to major brain dysfunction over time. There is no known cure for AD, and current treatments can only delay the illness's course. Early AD diagnosis allows people to learn about the condition and plan for future requirements. Also, symptom-delaying medications can be utilized whenever it is most convenient for the patient. A prompt diagnosis also reduces the overall cost of care. As a result, the only way to assure effective treatment is early identification [3–5].

Several brain imaging modalities, such as magnetic resonance imaging, positron emission tomography, single-emission computed tomography, and electroencephalogram (EEG), are utilized in computer-aided diagnosis systems to get information on the neurodegenerative process. During the last two decades, there has been significant growth in clinical and academic attention to EEG as a viable, non-invasive technique sensitive enough for neurological disease diagnosis and severity assessment [3, 5]. A loss in EEG complexity, a slowing of the EEG, and disruptions in EEG synchronization are some of the most prominent abnormalities in the EEG signals of AD patients. This inspired the researchers to create multiresolution analysis and feature extraction methods to examine the EEG data of AD patients [6]. In recent decades, several studies have

Preliminary results of this study was presented at the Medical Technologies Conference, TIPTEKNO'22, held on Oct. 31-Nov. 02, 2022, in Antalya, Turkey.

Corresponding author:
Ozlem Karabiber Cura

E-mail:
ozlem.karabiber@ikcu.edu.tr

Received: March 14, 2023

Revision Requested: July 14, 2023

Accepted: August 2, 2023

Publication Date: November 23, 2023

DOI: 10.5152/electrica.2023.23029

been conducted to automatically diagnose AD utilizing different combinations of time, frequency, time–frequency (TF), and nonlinear analysis approaches.

In order to detect EEG signals in dementia patients, several studies have examined the total power, absolute power, and relative power of different EEG frequency bands, such as delta (≤4 Hz), theta (4–8 Hz), alpha (8–13 Hz), beta (13–30 Hz), and gamma (≥30 Hz) [6–10]. According to earlier research, AD patients differed from cognitively healthy older people by having (i) higher variability and greater power in the delta (≤4 Hz) and theta (4–8 Hz) frequency bands and (ii) a slowdown in frequency and lower power in the alpha (8–13 Hz) frequency bands. Nonlinear features that are complexity-based such as entropy: approximate entropy [7, 8, 11, 12], spectral entropy [13], sample entropy [11], permutation entropy [11, 12, 14], Tsallis entropy [11], and fuzzy entropy [15]; fractal dimension: Higuchi [6, 13, 16] and Katz's [6, 16]; and Lyapunov exponent [17], Lempel–Ziv complexity [18, 19], zero crossing rate, spectral roll-off, spectral centroid [20], and Kolmogorov complexity [21] are computed from AD patients and control subjects (CS) in many studies. In each of these investigations, it was underlined that the brain complexity of AD patients was lower than that of the control group, and encouraging findings have been presented. Different decomposition techniques, including discrete wavelet transform [6, 20, 22–25], continuous wavelet transforms (CWTs) [26, 27], empirical mode decomposition (EMD) [22, 28], ensemble EMD [28], and iterative filtering decomposition [29], have also been employed for the analysis of EEG data of AD patients in addition to computing different features from EEG signals or their sub-bands.

Several of the handcrafted feature extraction approaches listed above have been proposed for AD EEG classification utilizing traditional machine learning (ML) algorithms (i.e., Support Vector Machine (SVM), Linear Discriminant Analysis (LDA), k-Nearest Neighbor (kNN), and Artificial Neural Networks (ANNs)) [8, 13, 22]. Whereas these manual feature extraction and ML-based models provided excellent classification results, they are computationally complex and difficult for physicians to understand. These issues are addressed by the suggested mixed deep learning (DL) approaches, which are based on EEG time-series data or their frequency domain or TF representations (TFRs) [30–33].

In this paper, using an advanced DL-based quantitative EEG processing technology, we present a novel method for the challenge of differentiating AD from CS.

II. PROPOSED METHOD

This research presents a unique TFR and deep feature extraction-based technique for detecting EEG segments in AD and CS patients. Fig. 1 provides the flowchart for the proposed technique. The processing modules are explained in the following:

- *N*-channel AD and CS EEG recording: A Philips Alice-6 device was used to record 19-channel EEG signals from 15 AD patients and 11 CS.
- Preprocessing: An expert system is used to eliminate the artifacts. The EEG recording is then divided into *N* non-overlapping epochs of 5 seconds, and each epoch is examined separately.
- Time–frequency representation of AD/CS EEG segments: Every EEG segment is transformed into the joint TF domain using short-time Fourier transform (STFT) and synchrosqueezing transform (SST). Given the *n*th epoch under study, the corresponding TFR for each EEG channel is calculated, yielding a total of 19 TFRs.
- Deep feature extraction: The deep learning model, ResNet50, is used for feature extraction, and
- Classification: Three traditional ML techniques are employed to discriminate between the EEG epochs of CS and AD patients, utilizing the deep feature set. To accomplish 2-way classification problems, multi-modal ML classifiers based on Decision Tree (DT), SVM, and kNN architectures are created.

A. Electroencephalogram Data Set of Alzheimer's Dementia

The EEG data from 15 AD patients identified with early-stage AD using diagnostic testing and neuroimaging, as well as 11 CS, are

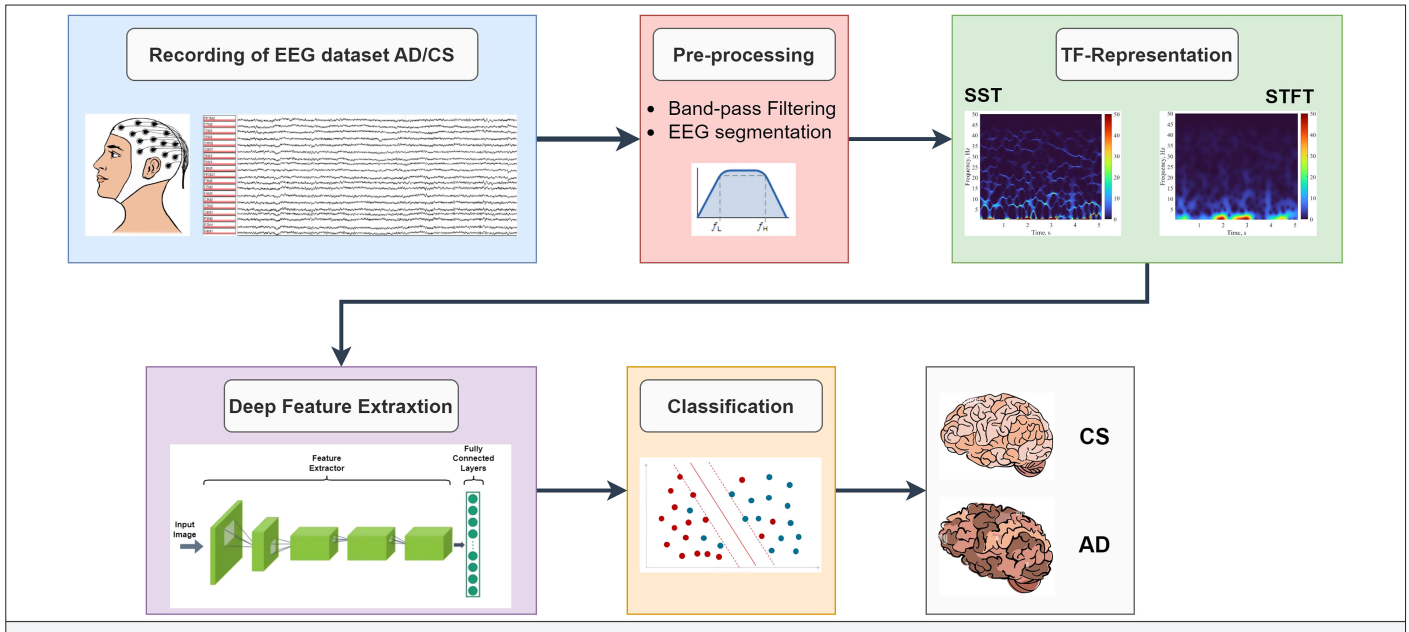

Fig 1. Proposed deep feature extraction-based classification of AD and CS EEG data is depicted in a flowchart. AD, Alzheimer's disease; CS, control subjects; EEG, electroencephalogram; SST, synchrosqueezing transform; STFT, short-time Fourier transform; TF, time–frequency.

collected using a Philips Alice-6 device with 19 channels and a sampling frequency of 200 Hz. The data collection was undertaken at the Faculty of Medicine's Neurology Department dementia clinic. For EEG signal recording, an international 10–20 electrode system with 19 channels (Fp1, F7, T3, T5, O1, O2, T6, T4, F8, Fp2, F3, Fz, F4, C3, Cz, C4, P3, Pz, and P4) was used. In order to record EEG data, the Clinical Research Ethics Committee granted ethical approval. Because the relevance of examining distinct brain clusters independently in AD is underlined [8], we examined different brain clusters in our study: anterior (Fp1, F3, Fz, Fp2, F4), posterior (P3, O1, Pz, P4, O2), central (C3, Cz, C4), temporal/left (T3, T5, F7), and temporal/right (T4, T6, F8).

B. Preprocessing

During the preprocessing stage, each EEG data is subjected to a Butterworth type II band-pass filter with a pass band of 0.5–40 Hz to reduce power line interference (50 Hz) and many other artifacts, such as the participants' muscle movement and eye blinking. The AD and CS EEG signals are then divided into non-overlapping windows with 1000 samples (5 seconds long; a total of 250 EEG segments for AD and CS groups for each channel). As a result, $250 \times 19 \times 15 = 71\,250$ EEG segments for AD patients and $250 \times 19 \times 11 = 52\,250$ EEG segments for CS are produced.

C. Time–Frequency Representation of Electroencephalogram segments

The classic TFR, the STFT, is efficiently employed in a variety of study domains, including signal analysis, digital image processing, voice processing, biology, and medicine, as well as EEG signal analysis. By moving the time window with some overlap, the signal is separated into numerous short-time segments in this approach, and the Fourier transforms of these short segments are computed. Windowing is the term for this procedure, and the window function "ω(·)" impacts the time and frequency resolution of the final TFR. In order to get greater temporal resolution, the narrow window function should be chosen, whereas a wide window function offers superior frequency resolution. The TF resolution is thus influenced by a variety of factors, including window type and length, frequency samples, and degree of overlap [34, 35]. The magnitude square of the STFT "$X(t, \omega)$" is calculated to produce the so-called "Spectrogram, $|X(t, \omega)|^2$", which is frequently used to determine how the signal's energy is distributed over a joint TF plane.

$$X(t,\omega) = \int_{-\infty}^{\infty} x(\tau)\omega(\tau - t)e^{-j\omega\tau}d\tau \quad (1)$$

where $X(t)$ indicates the analyzed signal; $X(t, \omega)$ denotes the STFT; and $\omega(t)$ is the window function.

The synchrosqueezing transform is part of the TF reassignment methods family, which was originally designed for audio data processing utilizing the CWT. Eventually, STFT-based SST (FSST) was introduced and utilized in a number of applications for signal analysis. The SST approximates the ideal TFR by raising the energy concentration of an initial TFR estimated using conventional procedures [36, 37].

The instantaneous frequency (IF) "$\omega_0(t, \omega)$" is calculated starting with the STFT "$X(t, \omega)$" as follows:

$$\omega_0(t,\omega) = -j\frac{1}{X(t,\omega)}\frac{\partial X(t,\omega)}{\partial t}$$

Synchrosqueezing transform reallocates the STFT coefficients' energy by merging STFT coefficients with the same instantaneous frequency information to improve frequency localization. Therefore, the FSST-based synchrosqueezing operator

"$\int_{-\infty}^{\infty} \delta(\eta - \omega_0(t,\omega))d\omega$"

and IF $\omega_0(t, \omega)$ are used to get the SST "$T(t, n)$" [37].

$$T(t,\eta) = \frac{1}{g(0)}\int_R X(t,\omega)\delta(\eta - \omega_0(t,\omega))d\omega \quad (2)$$

In this study, we employ TFRs obtained by FSST and STFT in our deep feature extraction-based technique for classifying AD/CS EEG segments. Fig. 2 depicts an example TFR of AD and CS generated by STFT and SST approaches for a 5-second EEG segment.

D. Deep Feature Extraction

In recent years, hybrid techniques based on deep learning and ML have become more prominent in EEG classification approaches. These methods include extracting features from the deep learning model and feeding them into ML algorithms as an input feature set. These hybrid techniques outperform ML and handcrafted-based feature extraction approaches in terms of speed, ability to handle difficult computational issues, and diagnostic accuracy [4]. In this study, to learn features from the TFR of EEG signals and categorize them into AD and CS classes using ML techniques, four pretrained Convolutional Neural Networks (CNN) models—AlexNet, ResNet18, ResNet50, and GoogleNet—are employed [38, 39].

One of the extensively used deep CNN architectures, AlexNet, has attracted a lot of interest in the field of artificial intelligence. It has 8 layers, 5 of which are convolutional and 3 of which are fully connected (FC). In order to extract features, the "fc8" layer is employed, and 1000-dimensional deep feature vectors are produced. The ResNet-18 architecture trains images quicker than others without losing performance. One 7×7 convolutional layer, two pool layers, five residual blocks, and one FC layer comprise this architecture. To extract features, the "fc1000" layer is employed, and 1000-dimensional deep feature vectors are generated [40]. ResNet-50 is a 50-layer residual CNN aimed at addressing the problem of disappearing gradients during back propagation by introducing shortcut links between conventional CNN networks. The fc1000 layer is used in the feature extraction procedure, and the extracted feature vector is 1000-dimensional [38, 39]. GoogleNet is a unique, tiny network that stands out from the others. The architecture is built using nine inception modules. The inception module is made up of a few tiny convolutional kernels (such as 1×1, 3×3, and 5×5), which help to reduce the number of parameters and complexity of the model [41]. The FC layer was used to extract the features, and the extracted feature vectors are 1000-dimensional.

Different images are used as input to train the CNN network in its design. Convolutional layers use filters to convolve input images in order to create feature maps. By retaining the high-level features, the pooling layer then reduces the size of the image. Finally, the fully connected layer is used to generate the results [40]. The proposed work feeds the CNN architecture with TF images acquired from AD

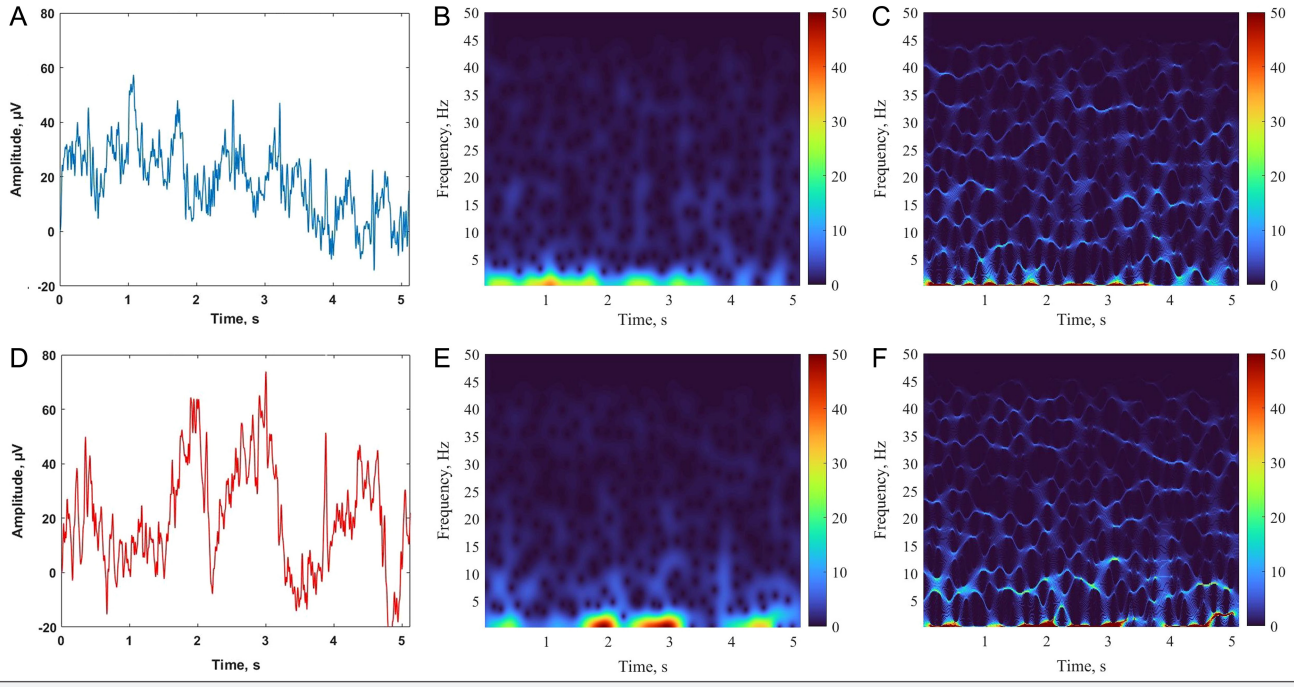

Fig 2. A 5-second electroencephalogram segment of (A) control subjects and (D) Alzheimer's disease, with time–frequency representations of (B, E) short-time Fourier transform and (C, F) synchrosqueezing transform.

and CS EEG segments utilizing SST and STFT techniques. The calculated TFRs are saved as 224 × 224 × 3 RGB color images. The TF image dataset is divided into 70% training images [for each channel, 2625 images for the AD class (70% of 250 × 15 images) and 1925 images for the CS class (70% of 250 × 11 images)] and 30% testing images [1125 images for the AD class (30% of 250 × 15 images) and 825 images for the CS class (30% of 250 × 11 images)].

E. Classification

Three separate classifiers, fine DT [8], linear SVM [13, 22, 31, 37], and weighted kNN [8, 22, 37], are used to classify the EEG segments of AD and CS in the proposed deep feature and TFR-based technique. To assess the performance of the suggested strategy, 10-fold cross-validation is used. Several statistical metrics, including accuracy (ACC), sensitivity (SEN), precision (PRE), and false discovery rate (FDR), are used to evaluate classifier performance [22, 31, 37].

III. EXPERIMENTAL RESULTS AND DISCUSSION

Deep feature extraction is performed utilizing four distinct CNN models, namely Resnet18, Resnet50, AlexNet, and GoogleNet, after the EEG segments' TFR is obtained using the STFT and SST approaches. Three classifiers—DT, SVM, and kNN—are then used to differentiate two groups of CS and AD. Classifications are performed for 19 EEG

TABLE I. THE PERFORMANCE EVALUATION RESULTS OF SST AND STFT-BASED TF APPROACHES IN DIFFERENT CNN MODELS AND CLASSIFIERS

		DT (%)			SVM (%)			kNN (%)		
Methods	**CNN Models**	**ACC**	**SEN**	**PRE**	**ACC**	**SEN**	**PRE**	**ACC**	**SEN**	**PRE**
	ResNet18	78.72	84.29	80.61	86.73	90.25	87.65	86.43	91.32	86.46
STFT	ResNet50	80.09	85.80	77.01	86.95	91.55	86.73	87.07	92.35	87.66
	AlexNet	77.70	82.33	73.91	84.08	90.20	84.50	84.94	90.68	85.54
	GoogleNet	76.93	82.28	74.55	83.97	86.34	85.32	82.10	87.12	82.27
	ResNet18	68.67	74.88	72.60	79.12	84.46	80.89	75.25	81.02	77.95
SST	ResNet50	72.85	79.23	67.16	81.59	88.15	80.56	80.02	86.39	78.12
	AlexNet	65.35	73.88	57.74	75.06	84.61	73.85	70.73	82.05	67.55
	GoogleNet	62.34	72.97	53.43	73.42	87.18	74.69	64.89	77.57	58.24

ACC, accuracy; DT, Decision Tree; kNN, k-Nearest Neighbor; PRE, precision; SEN, sensitivity; SST, synchrosqueezing transform; STFT, short-time Fourier transform; SVM, Support Vector Machine; TF, time–frequency.

TABLE II. RESULTS OF BRAIN CLUSTER-BASED CLASSIFICATION USING SST AND STFT TECHNIQUES FOR THE RESNET50 MODEL

		DT (%)			SVM (%)			kNN (%)		
Brain Cluster	**Method**	**ACC**	**SEN**	**PRE**	**ACC**	**SEN**	**PRE**	**ACC**	**SEN**	**PRE**
Anterior	STFT	80.94	86.21	80.19	87.77	92.14	88.68	87.10	92.12	88.46
	SST	74.98	80.50	71.96	83.87	89.03	83.79	81.46	85.97	79.94
Central	STFT	77.64	87.02	72.37	84.79	93.57	85.89	85.13	94.34	87.43
	SST	69.81	80.56	60.72	79.52	90.96	80.36	78.15	89.87	77.44
Temporal/Left	STFT	81.17	87.38	80.14	87.50	91.53	87.17	89.49	94.84	91.75
	SST	74.03	81.13	70.64	81.34	87.88	80.76	81.52	90.61	83.84
Temporal/Right	STFT	80.54	82.22	72.08	88.90	90.79	86.18	87.63	90.06	83.96
	SST	75.07	77.84	65.75	84.57	87.75	80.15	82.68	86.07	77.31
Posterior	STFT	79.81	85.85	77.69	85.93	90.23	85.34	86.43	91.26	86.76
	SST	70.51	76.87	64.96	78.92	85.97	77.60	77.22	82.37	73.78

ACC, accuracy; DT, Decision Tree; kNN, k-Nearest Neighbor; PRE, precision; SEN, sensitivity; SST, synchrosqueezing transform; STFT, short-time Fourier transform; SVM, Support Vector Machine; TF, time–frequency.

channels separately, and average performances are calculated for each classifier and CNN model.

MATLAB R2022b has been used to implement each experiment. According to the experimental results given in Table I, the ResNet50 model outperformed the other CNN models in all classifiers, obtaining an accuracy of up to 87.07% for the STFT approach and 81.59% for the SST approach. When all CNN models are considered, the SVM classifier yields the best average classification performances for most of the cases of both STFT and SST methods.

In order to show the effectiveness of the TF-based dementia diagnosis method, more detailed analyses are conducted utilizing the ResNet50 model, considering the results given in Table I.

Table II displays the results of performance evaluation according to three classifiers and two separate TFR approaches for each brain cluster (anterior, posterior, central, temporal/left, and temporal/right). With 89.49% ACC, 94.84% SEN, and 91.75% PRE from the temporal/left brain cluster, the STFT approach and kNN classifier perform the best in discriminating EEG segments of CS and AD patients. Moreover, Fig. 3 depicts the change in the average sensitivity and false discovery rate obtained by averaging the SEN and FDR values of the classifiers based on methods and brain clusters. The temporal/left brain region yields the greatest average SEN and lowest average FDR values (STFT: 91.25% SEN, 13.65% FDR; SST: 86.54% SEN, 21.59% FDR) for both STFT and SST techniques. The STFT strategy outperformed the SST approach in all brain clusters.

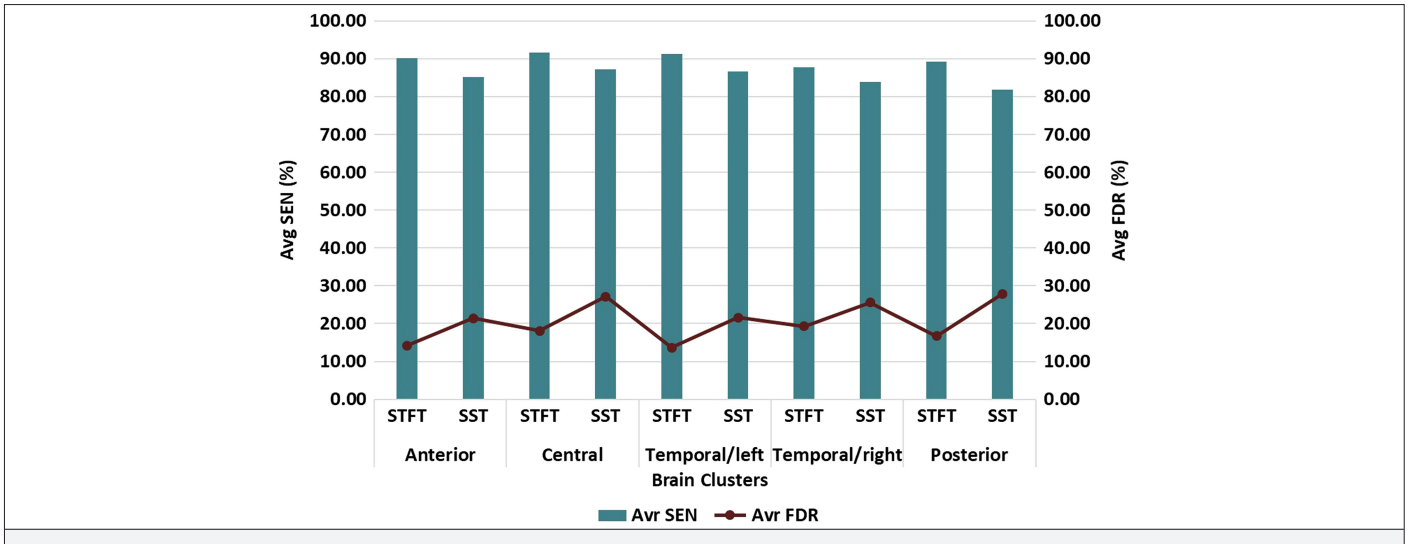

Fig 3. A comparison of the average sensitivity and false discovery rate values produced by STFT and SST methods, as well as the ResNet50 model, in accordance with distinct brain clusters. FDR, false discovery rate; SST, synchrosqueezing transform; STFT, short-time Fourier transform.

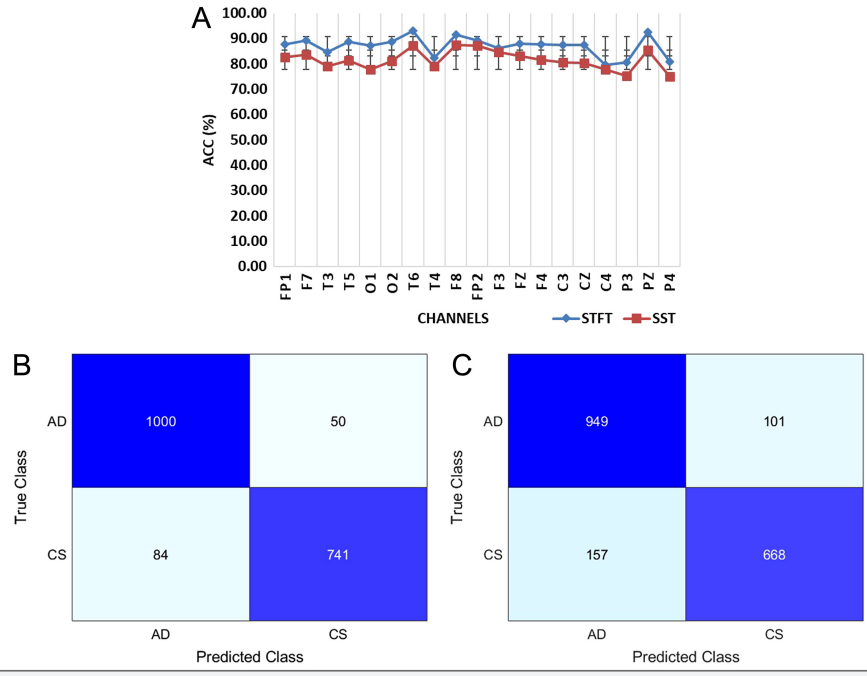

Fig 4. Channel-based accuracy values of STFT- and SST-based techniques achieved using the SVM classifier; confusion matrices created by the SVM classifier in the T6 channel for assessing the data of the (B) STFT and (C) SST methods. ACC, accuracy; AD, Alzheimer's disease; CS, control subjects; SST, synchrosqueezing transform; STFT, short-time Fourier transform.

Regarding Table II, it is worth noting that the SVM classifier outperforms both the SST and STFT techniques for almost all brain clusters. Fig. 4(A) shows the ACC values acquired for each channel using the SVM classifier in order to select the channels with the best CS/AD classification accuracy. The T6 channel provides the best AD/CS EEG segment classification accuracy for both methods (STFT: 92.96%, SST: 87.15%). Fig. 4(B)–(C) shows the confusion matrices obtained in Channel T6 from test pictures of the STFT and SST techniques using the SVM classifier. The P3 channel also provides the lowest accuracy (STFT: 80.46%, SST: 75.33%) in AD/CS EEG segment classification.

In addition to the above calculations, using the within-subject and cross-subject paradigms, classification accuracies are calculated to reveal the performance of the proposed approaches. During the within-subject paradigm, a subset of the data for each subject is utilized to train a model, and the remaining data are used for testing. So during training, the model has a chance to capture features that are typical of all subjects. In contrast, in the cross-subject paradigm, the model is trained using data from other subjects, and the model is tested using data from subjects that are not utilized in the model's training [33]. As a result, the classification accuracy indicates how well the model can be applied to all types of data. A comparison of the proposed model's classification accuracy for the within- and cross-subject paradigms and each brain cluster is shown in Fig. 5(A). In the within-subject paradigm, higher average classification accuracies ≥80 are obtained for all brain clusters; however, in the cross-subject paradigm, for all brain clusters, approximately 10%–15% lower average classification accuracies are obtained for each brain cluster. The model can only learn the properties of the subjects that are used for training in the cross-subject paradigm, as there is no possibility to exchange each subject's features for training and testing across subjects. As a result, the within-subject paradigm outperforms the cross-subject paradigm in average test accuracy. Fig. 5(B) shows the box plots representing the variation in test prediction accuracy of each individual in the cross-subject paradigm for each brain region. It is noteworthy that some subjects have high test accuracy, while others have low test accuracy. These findings suggest that the huge inter-subject differences in brain dynamics make it challenging to estimate the EEG segments of unknown subjects.

The results of our proposed model are compared with the most recent approaches used to diagnose AD by using EEG data. Table III shows some details about the studies and their experimental results. These approaches include classical feature engineering and ML-based methods [8, 13, 19, 20, 22, 28] as well as DL-based [30–33] methods. At the classification step, deep learning methods are classified into two types depending on the models used: hybrid ML- and deep learning-based (proposed methods) and CNN-based [30–33] methods. Although the datasets used in all of the publications are EEG datasets, the number of AD patients and CS utilized in various types of literature varies. While we employ a different number of subjects' datasets than the other literature, our technique obtains good performance regardless of whether the baseline literature uses more (e.g., [13]) or fewer (e.g., [32]) data. Some of the studies that used feature engineering and ML methods [20, 22, 28] provided higher accuracy values compared to those of the proposed method. However, calculating lots of features is mostly a time-consuming and tiring process. Comparing our results with approaches based on DL [30–33], it is seen that we have obtained almost similar or slightly lower success. Deep learning approaches, on the other hand, require a lengthy time to use in the classification stage due to their significant iteration time. However, our proposed method includes deep feature extraction and a ML-based classification stage. Therefore, the model is promising in terms of providing rapid analysis and high AD detection success.

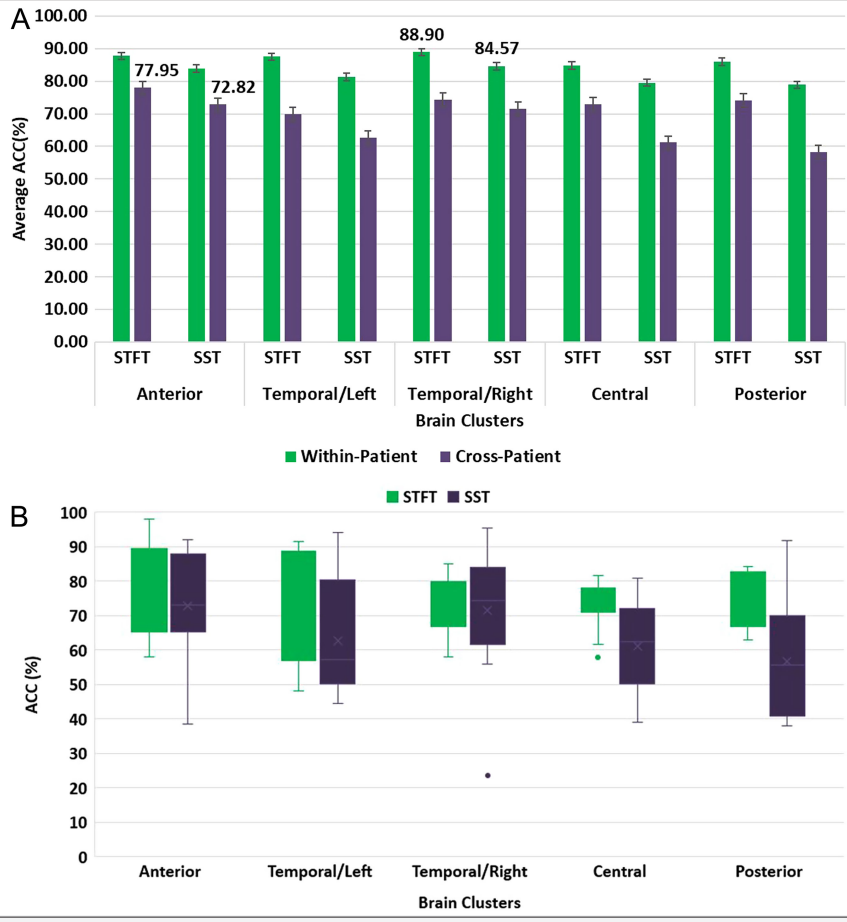

Fig 5. (A) Comparison of classification accuracy of proposed ResNet50-based model for within-subjects and cross-subjects' paradigm and (B) box plots depicting the accuracy patterns for each subject in the cross-subject paradigm for five brain clusters. ACC, accuracy; SST, synchrosqueezing transform; STFT, short-time Fourier transform.

TABLE III. PERFORMANCE EVALUATION OF CS VERSUS AD PATIENT EEG SIGNAL CATEGORIZATION STUDIES

Ref	Subjects Number	Feature	Classifier	Performance (%)
[8]	14 AD/10 CS	Statistical and spectral	ML	91.77% ACC
[20]	50 AD 50 CS	Wavelet-, spectral-, and complexity-based feature	ML	88%–96% ACC
[13]	79 AD/82 CS	Higuchi fractal dimension and spectral entropy	ML	66%–77% ACC
[22]	35 CS/20 AD	EMD and DWT-based features	ML	97.64% ACC
[19]	11 AD/11 CS	Lempel-Ziv complexity	ML	77.27%–78.25% ACC
[28]	15 AD/11 CS	EMD, EEMD, and DWT-based Features	ML	91.8%–95.2% ACC
[30]	63 AD/23 CS	CWT based TFR	CNN	85% ACC
[31]	63 AD/63 CS	PSD of EEG	CNN	81.41%–92.95% ACC
[32]	4 AD/4 CS	EEG spectral images	CNN	78.33%–95.04% ACC
[33]	39 AD/52 CS	Time domain EEG	CNN	98.7%–100% ACC
Proposed	15 AD/11 CS	STFT- and SST-based TFR	CNN + ML	79.56%–92.96% ACC

ACC, accuracy; AD, Alzheimer's disease; CNN, Convolutional Neural Networks; CWT, continuous wavelet transforms; CS, control subjects; DWT, discrete wavelet transform; EEMD, ensemble empirical mode decomposition; EMD, empirical mode decomposition; EEG, electroencephalogram; ML, machine learning; PSD, Power Spectral Density; SST, synchrosqueezing transform; STFT, short-time Fourier transform; TFR, time–frequency representation.

IV. CONCLUSION

A deep feature extraction strategy based on TFRs of EEG segments is described in order to classify AD patients and control participants. To generate TFRs of EEG data, a traditional TF approach, STFT, and the currently discovered SST method, which ensures superior resolution in the combined TF domain, are utilized. The resulting TFRs are treated as color images and fed into the Resnet-50 CNN architecture. The CNN model is used to extract deep features, which are subsequently classified using three popular ML algorithms: DT, SVM, and kNN. Short-time Fourier transform, which generally produces poor TF localization owing to fixed bandwidth analysis, outperformed the highly localized SST method in categorizing EEG segments of AD patients and control individuals.

Calculating informative features for ML algorithms takes time and frequently results in computational costs. A promising alternative to manual feature extraction is automatic feature extraction by deep networks. Deep learning approaches, on the other hand, require a long time in the classification stage due to their lengthy iteration time. As a result, this study provides a hybrid technique for classifying AD and CS EEG segments that combine deep TF feature extraction with standard ML algorithms for classification.

Peer-review: Externally peer-reviewed.

Author Contributions: Concept – O.K.C., A.A.; Design – O.K.C., H.S.T.; Supervision – A.A.; Funding – A.A.; Materials – O.K.C., H.S.T.; Data Collection and/or Processing – O.K.C.; Analysis and/or Interpretation – O.K.C., A.A.; Literature Review – O.K.C., A.A.; Writing – O.K.C., A.A.; Critical Review – H.S.T., A.A.

Declaration of Interests: The authors have no conflict of interest to declare.

Funding: The authors declared that this study has received no financial support.

REFERENCES

1. G. M. Savva *et al.*, "Prevalence, correlates and course of behavioural and psychological symptoms of dementia in the population," *Br. J. Psychiatry*, vol. 194, no. 3, pp. 212–219, 2009. [CrossRef]
2. M. Cantone *et al.*, "The contribution of transcranial magnetic stimulation in the diagnosis and in the management of dementia," *Clin. Neurophysiol.*, vol. 125, no. 8, pp. 1509–1532, 2014. [CrossRef]
3. A. Ortiz, J. Munilla, J. M. Gorriz, and J. Ramirez, "Ensembles of deep learning architectures for the early diagnosis of the Alzheimer's disease," *Int. J. Neural Syst.*, vol. 26, no. 7, p. 1650025, 2016. [CrossRef]
4. B. A. Mohammed *et al.*, "Multi-method analysis of medical records and MRI images for early diagnosis of dementia and Alzheimer's disease based on deep learning and hybrid methods," *Electronics*, vol. 10, no. 22, p. 2860, 2021. [CrossRef]
5. M. Şeker, Y. Özbek, G. Yener, and M. S. Özerdem, "Complexity of EEG dynamics for early diagnosis of Alzheimer's disease using permutation entropy neuromarker," *Comput. Methods Programs Biomed.*, vol. 206, p. 106116, 2021. [CrossRef]
6. D. V. Puri, S. L. Nalbalwar, A. B. Nandgaonkar, J. P. Gawande, and A. Wagh, "Automatic detection of Alzheimer's disease from EEG signals using low-complexity orthogonal wavelet filter banks," *Biomed. Signal Process. Control*, vol. 81, p. 104439, 2023. [CrossRef]
7. D. Abásolo, R. Hornero, P. Espino, J. Poza, C. I. Sánchez, and R. de la Rosa, "Analysis of regularity in the EEG background activity of Alzheimer's disease patients with approximate entropy," *Clin. Neurophysiol.*, vol. 116, no. 8, pp. 1826–1834, 2005. [CrossRef]
8. K. D. Tzimourta *et al.*, "EEG window length evaluation for the detection of Alzheimer's disease over different brain regions," *Brain Sci.*, vol. 9, no. 4, p. 81, 2019. [CrossRef]
9. A. I. Triggiani *et al.*, "Classification of healthy subjects and Alzheimer's disease patients with dementia from cortical sources of resting state EEG rhythms: A study using artificial neural networks," *Front. Neurosci.*, vol. 10, p. 604, 2016. [CrossRef]
10. F. Miraglia *et al.*, "Small world index in default mode network predicts progression from mild cognitive impairment to dementia," *Int. J. Neural Syst.*, vol. 30, no. 2, p. 2050004, 2020. [CrossRef]
11. K. D. Tzimourta *et al.*, "Analysis of electroencephalographic signals complexity regarding Alzheimer's disease," *Comput. Electr. Eng.*, vol. 76, pp. 198–212, 2019. [CrossRef]
12. L. Tylová, J. Kukal, V. Hubata-Vacek, and O. Vyšata, "Unbiased estimation of permutation entropy in EEG analysis for Alzheimer's disease classification," *Biomed. Signal Process. Control*, vol. 39, pp. 424–430, 2018. [CrossRef]
13. T. Staudinger, and R. Polikar, "Analysis of complexity based EEG features for the diagnosis of Alzheimer's disease," in 2011 Annual International Conference of the IEEE Engineering in Medicine and Biology Society. IEEE, pp. 2033–2036, 2011. [CrossRef]
14. N. Mammone, C. Ieracitano, H. Adeli, A. Bramanti, and F. C. Morabito, "Permutation Jaccard distance-based hierarchical clustering to estimate EEG network density modifications in MCI subjects," *IEEE Trans. Neural Netw. Learn. Syst.*, vol. 29, no. 10, pp. 5122–5135, 2018. [CrossRef]
15. S. Simons, P. Espino, and D. Abásolo, "Fuzzy entropy analysis of the electroencephalogram in patients with Alzheimer's disease: Is the method superior to sample entropy?," *Entropy (Basel)*, vol. 20, no. 1, p. 21, 2018. [CrossRef]
16. J. P. Amezquita-Sanchez, N. Mammone, F. C. Morabito, S. Marino, and H. Adeli, "A novel methodology for automated differential diagnosis of mild cognitive impairment and the Alzheimer's disease using EEG signals," *J. Neurosci. Methods*, vol. 322, pp. 88–95, 2019. [CrossRef]
17. J. Jeong, S. Y. Kim, and S. H. Han, "Non-linear dynamical analysis of the EEG in Alzheimer's disease with optimal embedding dimension," *Electroencephalogr. Clin. Neurophysiol.*, vol. 106, no. 3, pp. 220–228, 1998. [CrossRef]
18. D. Abásolo, R. Hornero, C. Gómez, M. García, and M. López, "Analysis of EEG background activity in Alzheimer's disease patients with lempel–ziv complexity and central tendency measure," *Med. Eng. Phys.*, vol. 28, no. 4, pp. 315–322, 2006. [CrossRef]
19. S. Simons, and D. Abásolo, "Distance-based lempel–ziv complexity for the analysis of electroencephalograms in patients with Alzheimer's disease," *Entropy*, vol. 19, no. 3, p. 129, 2017. [CrossRef]
20. N. N. Kulkarni, and V. K. Bairagi, "Extracting salient features for EEG-based diagnosis of Alzheimer's disease using support vector machine classifier," *IETE J. Res.*, vol. 63, no. 1, pp. 11–22, 2017. [CrossRef]
21. D. Puri, S. Nalbalwar, A. Nandgaonkar, and A. Wagh, "Eeg-based diagnosis of Alzheimer's disease using Kolmogorov complexity," in *Applied Information Processing Systems*. Berlin: Springer, 2022, pp. 157–165. [CrossRef]
22. M. S. Safi, and S. M. M. Safi, "Early detection of Alzheimer's disease from EEG signals using Hjorth parameters," *Biomed. Signal Process. Control*, vol. 65, p. 102338, 2021. [CrossRef]
23. V. Bairagi, "EEG signal analysis for early diagnosis of Alzheimer disease using spectral and wavelet based features," *Int. J. Inf. Technol.*, vol. 10, no. 3, pp. 403–412, 2018. [CrossRef]
24. F. Berte', G. Lamponi, R. S. Calabro', and P. Bramanti, "Elman neural network for the early identification of cognitive impairment in Alzheimer's disease," *Funct. Neurol.*, vol. 29, no. 1, p. 57–65, 2014.
25. B. Oltu, M. F. Akşahin, and S. Kibaroğlu, "A novel electroencephalography based approach for alzheimer's disease and mild cognitive impairment detection," *Biomed. Signal Process. Control*, vol. 63, p. 102223, 2021. Available: https://www.sciencedirect.com/science/article/pii/S1746809420303530
26. P. Durongbhan *et al.*, "A dementia classification framework using frequency and time-frequency features based on eeg signals," *IEEE Trans. Neural Syst. Rehabil. Eng.*, vol. 27, no. 5, pp. 826–835, 2019. [CrossRef]
27. C. Ieracitano, N. Mammone, A. Hussain, and F. C. Morabito, "A novel multi-modal machine learning based approach for automatic classification of eeg recordings in dementia," *Neural Netw.*, vol. 123, pp. 176–190, 2020. [CrossRef]
28. O. K. Cura, A. Akan, G. C. Yilmaz, and H. S. Ture, "Detection of Alzheimer's dementia by using signal decomposition and machine learning methods," *Int. J. Neural Syst.*, vol. 250, p. 2250042, 2022.

29. N. Sharma, M. H. Kolekar, and K. Jha, "Iterative filtering decomposition based early dementia diagnosis using eeg with cognitive tests," *IEEE Trans. Neural Syst. Rehabil. Eng.*, vol. 28, no. 9, pp. 1890–1898, 2020. [CrossRef]
30. F. C. Morabito *et al.*, "Deep convolutional neural networks for classification of mild cognitive impaired and Alzheimer's disease patients from scalp EEG recordings," in 2016 IEEE 2nd International Forum on Research and Technologies for Society and Industry Leveraging a better tomorrow (RTSI). IEEE, 2016, pp. 1–6. [CrossRef]
31. C. Ieracitano, N. Mammone, A. Bramanti, A. Hussain, and F. C. Morabito, "A convolutional neural network approach for classification of dementia stages based on 2D-spectral representation of EEG recordings," *Neurocomputing*, vol. 323, pp. 96–107, 2019. [CrossRef]
32. X. Bi, and H. Wang, "Early Alzheimer's disease diagnosis based on EEG spectral images using deep learning," *Neural Netw.*, vol. 114, pp. 119–135, 2019. [CrossRef]
33. J. Park *et al.*, "Individualized diagnosis of preclinical Alzheimer's disease using deep neural networks," *Expert Syst. Appl.*, vol. 210, p. 118511, 2022. [CrossRef]
34. C. Mateo, and J. A. Talavera, "Analysis of atrial and ventricular premature contractions using the short time fourier transform with the window size fixed in the frequency domain," *Biomed. Signal Process. Control*, vol. 69, p. 102835, 2021. [CrossRef]
35. R. Ramos-Aguilar, J. A. Olvera-Lo´pez, I. Olmos-Pineda, and S. Sa´nchez-Urrieta, "Feature extraction from EEG spectrograms for epileptic seizure detection," *Pattern Recognit. Lett.*, vol. 133, pp. 202–209, 2020. [CrossRef]
36. G. Yu, M. Yu, and C. Xu, "Synchroextracting transform," *IEEE Trans. Ind. Electron.*, vol. 64, no. 10, pp. 8042–8054, 2017. [CrossRef]
37. S. Mamli, and H. Kalbkhani, "Gray-level co-occurrence matrix of fourier synchro-squeezed transform for epileptic seizure detection," *Biocybern. Biomed. Eng.*, vol. 39, no. 1, pp. 87–99, 2019. [CrossRef]
38. N. Shajil, M. Sasikala, and A. M. Arunnagiri, "Deep learning classification of two-class motor imagery eeg signals using transfer learning," in 2020 International Conference on e-Health and Bioengineering (EHB). IEEE, 2020, pp. 1–4. [CrossRef]
39. F. Demir, N. Sobahi, S. Siuly, and A. Sengur, "Exploring deep learning features for automatic classification of human emotion using eeg rhythms," *IEEE Sens. J.*, vol. 21, no. 13, pp. 14923–14930, 2021. [CrossRef]
40. S. Misra, S. Jeon, S. Lee, R. Managuli, I.-S. Jang, and C. Kim, "Multi-channel transfer learning of chest X-ray images for screening of COVID-19," *Electronics*, vol. 9, no. 9, p. 1388, 2020. [CrossRef]
41. A. Benali Amjoud, and M. Amrouch, "Convolutional neural networks backbones for object detection," in Image and Signal Processing: 9th International Conference, ICISP 2020, June 4–6, 2020. Marrakesh, Morocco: Springer, 2020, pp. 282–289.

Ozlem Karabiber Cura received her B.Sc. degree in Biomedical Engineering from Erciyes University, Turkey, in 2014, and the Ph.D. degree from the Department of Biomedical Technologies, Izmir Katip Celebi University, in 2021. She has been working as an Assistant Professor at the Izmir Katip Celebi University, Department of Biomedical Engineering, since 2023. Her research interests include biomedical signal and image processing and applications of ML and deep learning methods for the detection and classification of biomedical signals.

Hatice Sabiha Ture graduated with a M.D. degree in 1997 from Dokuz Eylul University Faculty of Medicine, Turkey. In 2006, she received her specialization in the Department of Neurology at the Izmir Training and Research Hospital. Since 2020, she has held the position of Associate Professor in the Department of Neurology at Izmir Katip Celebi University. Her research interests include identifying the clinical and demographic characteristics of Parkinson's, epilepsy, multiple sclerosis, and ADs, as well as approaches for their early diagnosis and treatment.

Aydin Akan Aydin Akan received the B.Sc. degree from the University of Uludag, Bursa, in 1988, the M.Sc. degree from the Technical University of Istanbul, Turkey, in 1991, and the Ph.D. degree from the University of Pittsburgh, Pittsburgh, PA, USA, in 1996, all in Electronics Engineering. He has been with the Department of Electrical and Electronics Engineering, Istanbul University, between 1996 and 2017, where he was granted an Associate Professor position in 2001 and Professor position in 2006.

Currently, he is a Professor and Chair of the Department of Electrical and Electronics Engineering, at Izmir University of Economics. His current research interests include nonstationary signal processing, TF signal analysis, and ML methods applied to wireless communications and biomedical engineering. He is a senior member of the IEEE Signal Processing (SP) and Engineering in Medicine and Biology (EMB) Societies, Chair of IEEE-EMB Turkey Section, and member of the European Signal Processing Association (EURASIP) Biomedical Image and Signal Analytics (BISA) Technical Area Committee. He is an Associate Editor of the Elsevier Digital Signal Processing Journal.